Redox Biology 17 (2018) 411–422

Contents lists available at ScienceDirect

Redox Biology

journal homepage: www.elsevier.com/locate/redox

Research paper

Loss of the ubiquitin conjugating enzyme UBE2E3 induces cellular senescence

Kendra S. Plafker[a], Katarzyna Zyla[a], William Berry[b], Scott M. Plafker[a,c,*]

[a] Aging and Metabolism Research Program, Oklahoma Medical Research Foundation, Oklahoma City, OK, USA
[b] Department of Surgery, University of Oklahoma Health Sciences Center, Oklahoma City, OK, USA
[c] Department of Cell Biology, University of Oklahoma Health Sciences Center, Oklahoma City, OK, USA

ARTICLE INFO

Keywords:
UBE2E3
Senescence
Autophagy
Ubiquitin
Mitochondria

ABSTRACT

Cellular senescence plays essential roles in tissue homeostasis as well as a host of diseases ranging from cancers to age-related neurodegeneration. Various molecular pathways can induce senescence and these different pathways dictate the phenotypic and metabolic changes that accompany the transition to, and maintenance of, the senescence state. Here, we describe a novel senescence phenotype induced by depletion of UBE2E3, a highly-conserved, metazoan ubiquitin conjugating enzyme. Cells depleted of UBE2E3 become senescent in the absence of overt DNA damage and have a distinct senescence-associated secretory phenotype, increased mitochondrial and lysosomal mass, an increased sensitivity to mitochondrial and lysosomal poisons, and an increased basal autophagic flux. This senescence phenotype can be partially suppressed by co-depletion of either p53 or its cognate target gene, $p21^{CIP1/WAF1}$, or by co-depleting the tumor suppressor $p16^{INK4a}$. Together, these data describe a direct link of a ubiquitin conjugating enzyme to cellular senescence and further underscore the consequences of disrupting the integration between the ubiquitin proteolysis system and the autophagy machinery.

1. Introduction

Cellular senescence has emerged as a critical mechanism by which organisms suppress tumor proliferation and maintain tissue homeostasis and optimal wound healing. Paradoxically, the transition of cells to a state of senescence in particular anatomical niches has been implicated in the development of age-related neurodegenerative diseases [4]. The recognition of these dual roles for senescence has led to in-depth investigations of the pathways that drive proliferating cells, or those that are differentiated but have retained a proliferative potential, and even post-mitotic neurons [18] into an irreversible cell cycle arrest and senescence. These studies have uncovered numerous mechanisms by which senescence can be induced and maintained. The pathways range from genomic damage and the accompanying DNA damage response (DDR) to mitochondrial dysfunction associated senescence (MiDAS) to oncogene-induced senescence (OIS) [47]. Perhaps one of the most intriguing facets of how cells become senescent is that the metabolic and phenotypic changes that ensue differ depending on the initiating event. For example, a distinguishing hallmark of DDR-mediated senescence is a senescence-associated secretory phenotype (SASP) characterized by activation of IL-1β, NF-κB, IL-6 and their respective downstream signaling pathways. Yet, this inflammatory arm is not a prominent component of cells that become senescent through MiDAS, which is distinguished by a blunted inflammatory arm of SASP and expression of IL-10, CCL27, and AREG [48].

The ubiquitin (Ub) proteasome system (UPS) is comprised of a network of enzymes and activities that collectively regulate the stability, localization, and function of many intracellular proteins. The central protein of the UPS is Ub, a highly conserved, 76 amino acid polypeptide that is post-translationally conjugated onto cognate substrates. The attachment of Ub to target proteins is mediated by a hierarchal cascade of enzymes consisting minimally of a Ub-activating enzyme (E1), a Ub-conjugating enzyme (E2), and a Ub protein ligase (E3). The human genome encodes 2 E1s, 40–60 E2s, and 600–1000 E3s and substrate selection is conferred through the pairing of particular E2-E3 combinations (reviewed in [50]). *In vitro* and in vivo evidence established that a single E2 can partner with multiple E3s and vice versa. E3s can be single proteins or multi-subunit complexes.

Over the past decade, additional factors have been identified that facilitate the specificity of Ub conjugation to substrates but the E1-E2-

* Corresponding author.
E-mail address: plafkers@omrf.org (S.M. Plafker).

https://doi.org/10.1016/j.redox.2018.05.008
Received 18 April 2018; Received in revised form 17 May 2018; Accepted 18 May 2018
Available online 21 May 2018

E3 axis constitutes the core machinery. Akin to kinases and phosphatases, the ubiquitylation of substrates is countered by the trimming action of de-ubiquitylating enyzmes (DUBs). These enzymes, which are either thiol proteases or metalloenzymes, deconstruct Ub chains and thereby counter the synthetic activity of the E1-E2-E3 conjugation machinery. Substrates can be modified with monoUb or with polyUb chains or with both, and the consequences of ubiquitylation are in turn governed by factors including the number of Ub molecules attached, their configuration and topology, and the binding proteins that recognize monoUb and different forms of polyUb [21,43,49]. The best-studied consequence of polyUb synthesis on target substrates is to deliver the marked protein to the 26 S proteasome for degradation. The 26 S proteasome is a macromolecular assembly of proteases that cleaves substrates to peptides. The resulting peptide fragments are cleaved by cytoplasmic peptidases into amino acids or consumed *en bulk* for hydrolysis by the lysosome.

Over the past decade, studies have converged to reveal that ubiquitylation and the autophagy system cooperate to target damaged and dysfunctional organelles as well as invading bacteria for degradation via the autophagy-lysosomal system (reviewed in [12]). For example, the UPS E3 ligase parkin and its activating partner kinase, PINK1, have been shown to decorate damaged mitochondria with polyUb chains that serve as an initiating signal for elimination of these organelles by a specialized type of autophagy termed mitophagy (reviewed in [16,27]). This and similar discoveries highlight the extent to which Ub integrates the UPS and autophagy systems, and it is within this context that we have been investigating the metazoan enzyme, UBE2E3.

UBE2E3 is an E2 that partners with multiple E3 ligases to conjugate monoUb onto substrates [28]. The enzyme is highly conserved; the mouse and human protein sequences are identical. We reported an essential role for UBE2E3 in cell proliferation as knockdown of the enzyme causes a robust increase in $p27^{Kip1}$ and an accompanying cell cycle exit [32]. More recently, we demonstrated that depletion of the enzyme causes a dramatic redistribution of the normally reticular mitochondrial network [34]. This collapse of the mitochondrial network into a perinuclear tangle is accompanied by a re-localization of the anti-stress transcription factor Nrf2 from the nucleus to the mitochondrial tangle and a concomitant decrease in Nrf2 transcriptional activity [34]. Because cell cycle exit, disruption of mitochondrial homeostasis [48], and mis-localization of Nrf2 [22] have all been independently associated with cellular senescence and premature aging, and are all induced by UBE2E3 knockdown [32–34], we investigated whether the loss of UBE2E3 can drive proliferating cells into senescence.

Here we report that cellular senescence resulting from depletion of UBE2E3 is independent of DNA damage and is characterized by a distinct SASP profile, an increase in mitochondrial and lysosomal mass, a dependence on the expression of the tumor suppressor $p16^{INK4a}$ and on the nuclear expression of p53 and $p21^{CIP1/WAF1}$, and an increased basal autophagic flux. This senescence signature is distinguished from the previously defined DDR, OIR, and MIDAS senescence pathways. Moreover, this work provides the first direct evidence that suppressing the expression of a specific metazoan ubiquitin conjugating enzyme causes cellular senescence.

2. Materials and methods

2.1. Cell culture, siRNA transfections, stable cell lines, starvation

RPE-1 cells were cultured and transfected as described [30] and stable cell lines were constructed as described [30]. RPE-1 cells stably expressing GFP-LC3 were starved in Krebs-Ringer Solution containing Sodium Bicarbonate (Alfa Aesar cat# J67591) and 1 × Pen/Strep for 2 h.

Cell Line	Plasmid	Selection
Mito-Tomato		Puromycin
Mt-mKeima	pCHAC-mt-mKeima was a gift from Richard Youle (Addgene plasmid # 72342)	
GFP-LC3	pBABEpuro GFP-LC3 was a gift from Jayanta Debnath (Addgene plasmid # 22405)	Puromycin
roGFP	Gift from S. James Remington (Univ of Oregon)	Puromycin
Mito-roGFP	Gift from S. James Remington (Univ of Oregon)	Puromycin

2.2. Reagents, chemicals, siRNA, and antibodies

Antibody	Catalog#	Company	IF dilution	Western dilution
LaminB1	Ab16048	ABCAM	1:1000	
pH2A.X S139	05–636	Millipore	1:5000	
p53	SC-126	Santa Cruz	1:1000	1:1000
p-p53 Ser15	9284	Cell Signaling		1:1000
$p21^{CIP1/WAF1}$	2947	Cell Signaling	1:1000	
Actin-HRP	HRP-60008	Proteintech		1:20,000
HMBG1	Ab18256	ABCAM		1:1000

Chemical	Catalog#	Company	Concentration
Etoposide	E1383	Sigma	25 μM
Hydrogen Peroxide	95321	Sigma	1 mM
FCCP	BML-CM120	Enzo Life Sciences	5 μM
TMRE	70016	Biotium	5 nM
MitoTracker Green	M7514	ThermoFisher	200 nM
AndyFluor488 Annexin V	A034	Genecopoeia	5 μg/ml
Lysotracker Red	L7528	ThermoFisher	50 nM
Chloroquine	sc − 205629	Santa Cruz	50 μM

siRNA	Catalog #	Company
siControl	D-001220-01-20	Dharmacon
siUBE2E3	D-008845-02/D-008845-03	Dharmacon
sip53	Sc-29435	Santa Cruz
$sip21^{CIP/WAF1}$	6456	Cell Signaling
$sip16^{INK4a}$	DRHNO-000001	Dharmacon

2.3. Measurement of secreted IL-6

Human IL-6 Quantikine ELISA Kit (Cat# D-6050 R&D Systems) was used as per the manufacturer's recommendation to measure the secreted IL-6 in the media from 400,000 cells over 24 h, 10 days post treatment.

2.4. Immunofluorescence

Immunofluorescence analyses were done as described previously [30]. For visualizing lysosomal content and distribution, RPE-1 cells were treated with siRNA and 3 days later, incubated with 50 nM Lysotracker Red for 30 min and then imaged live on a Nikon TE2000 inverted microscope.

2.5. β-galactosidase and Edu labeling of cells

2–5 days post-treatment, 10 μM Edu was added and incubated at 37 °C for 24 h. Cells were stained for Senescence Associated Beta-galactosidase (β-gal) as per manufacturer's recommendation for 18 h (Catalog# K320-250; Biovision, Inc.). Cells were then permeabilized with 0.5% TX-100/PBS at room temperature for 5 min followed by incubation with Click-it Alexa 488 azide (Cat# C10337 ThermoFisher) and Hoechst 33342 solution.

2.6. qPCR

qPCR was performed as described in [34]. The primers were as follows:

$p16^{INK4a}$for – caacgcaccgaatagttacg; $p16^{INK4a}$rev – accagcgtgtccaggaag

Lamin B1 for – aggatcagattgcccagttg; Lamin B1 rev – tgcttccttctggtctcgtt

IL1β BioRad PrimePCR Unique Assay (ID# qHsaCID0022272); IL8 BioRad PrimePCR Unique Assay ID# qHsaCED0046633; CXCL1 BioRad PrimePCR Unique Assay ID# qHsaCED0046130; IL6 BioRad PrimePCR Unique Assay ID# qHsaCID0020314; CXCL2 BioRad PrimePCR Unique Assay ID# qHsaCED0057058; IL10 BioRad PrimePCR Unique Assay ID# qHsaCED0003369

2.7. Western blotting

Western blotting was done as described previously [30].

2.8. Flow cytometry assays

FlowJo 10.3 software was used for gating analysis and quantification for all flow cytometry studies.

a. Assessment of redox stress – RPE-1 cells stably expressing roGFP or mito-roGFP were siRNA transfected and 6 days later processed for flow cytometry using the 405 nm laser with 525/50 nm filter to visualize the oxidized roGFP and the 488 nm laser with 530/30 nm filter to visualize reduced roGFP.
b. Assessment of mitochondrial membrane potential – RPE-1 cells were co-labeled 6 days post-siRNA treatment with 5 nM tetramethylrhodamine, ethyl ester (TMRE) and 200 nM MitoTracker Green™ (MTG) for 30 min. Cells were trypsinized, resuspended in complete media lacking Phenol Red, filtered through 100 μm mesh and processed on a Beckton Dickinson LSR II. The MTG was visualized with the 488 nm laser with a 510/21 nm filter. TMRE was visualized with the 561 nm laser and a 582/15 nm filter. Membrane potential changes were calculated using the ratio between the red and green signals.
c. Assessment of cell death – Annexin V labeling 3 days post transfection, RPE-1 cells were treated with 5 μM FCCP or 50 μM chloroquine (CQ) for 24 h before being trypsinized, incubated in 5 μg/ml Andy Fluor488 Annexin V in Annexin Binding Buffer (ABB; 10 mM HEPES, pH 7.4; 140 mM NaCl; 2.5 mM $CaCl_2$) for 15 min, protected from light. The Annexin V solution was diluted 1:5 before being filtered and processed for flow cytometry using the same settings as the TMRE/MTG assay.
d. Measurement of mitochondrial mass – Mito-Tomato/MTG co-labeling was performed 6 days post-transfection on RPE-1 cells stably expressing mito-tdTomato and incubated with 200 nM MTG for 30 min before being processed for flow cytometry as described for the TMRE/MTG assay.
e. Mitophagy assay – RPE-1 cells stably expressing mitochondria-targeted (mt)-mKeima were processed as described previously [30]. Notably, the cells used in this manuscript were not over-expressing YFP-Parkin.
f. Assessment of lysosomal mass – LysoTracker Red (LTR) and Forward Scatter (FSC) were assessed 6 days post-transfection in RPE-1 cells incubated with 50 nM LTR for 30 min. Cells were resuspended in PBS + 2% fetal calf serum (FCS) and subjected to flow cytometry using the 561 nm laser and 582/15 nm filter. LTR intensity was graphed against FSC-A to account for the increased size of the siUBE2E3 and etoposide treated cells.
g. Acridine orange assay – To assess acidic vesicle mass, RPE-1 cells that had been transfected 6 days prior were subjected to flow cytometry with Acridine Orange as described previously [45].
h. Measurement of vesicle-associated GFP-LC3 – RPE-1 cells stably transfected with GFP-LC3 were transfected with siRNA. 3 days later they were treated with 5 μM FCCP, 50 μM CQ, or starved of amino acids and growth factors. Cells were then trypsinized, resuspended in 0.05% Saponin/PBS, pelleted at 500 × *g* for 5 min, resuspended in PBS, filtered and subjected to flow cytometry as described [13].

3. Results

Senescent cells are a hallmark of aging and have been linked to linked many age-related pathologies including cardiovascular disease, cancer, and neurodegeneration [5]. As senescent cells and Ub-positive aggregates are both prevalent features of neurodegenerative diseases such as Parkinson's disease (PD), Alzheimer's disease (AD) and Huntington's disease (HD), a disruption of the UPS machinery and Ub homeostasis might underlie or contribute to pathological senescence in certain physiological situations. To begin testing this idea, we depleted the highly conserved, metazoan Ub conjugating enzyme, UBE2E3, from human retinal pigment epithelial (RPE-1) cells. These cells are non-transformed, have a modal chromosome count of 46, are immortalized with telomerase, and reproducibly yield knockdown efficiency of UBE2E3 by 70–80% at the mRNA level [34]. We previously reported that knockdown of UBE2E3 induces a cell cycle exit [32], a disruption of mitochondrial homeostasis [34], and a reduction in the activity of the master anti-stress transcription factor Nrf2 [34]. As all three phenotypes are linked to senescence and premature aging [17], we subjected cells depleted of the enzyme (hereafter referred to as “siUBE2E3 cells”) to a panel of assays to assess cellular senescence.

6 days post-siRNA administration, siUBE2E3 cells took on a large, flattened appearance similar to etoposide (Etop)-treated cells (Fig. 1A). Etop is a DNA-damaging agent and a potent inducer of senescence [25,44]. We therefore used it as a positive control for senescence throughout this study. Depletion of UBE2E3 led to (1) a loss of proliferation, as indicated by a failure of siUBE2E3 cells to incorporate 5-ethynyl-2′-deoxyuridine (Edu), a marker of newly-synthesized DNA (Fig. 1B), (2) an increase in cell size [32], (3) a robust expression of senescence-associated β-galactosidase (SA-β-gal) (Fig. 1C), (4) a decrease in intracellular HMGB1 content (Fig. 1D), (4) redistribution of lamin B from its primary localization at the nuclear envelope (Fig. 1E, left panel) to a punctate, nucleoplasmic distribution (Fig. 1E, right panel) and a concomitant decrease in lamin B1 mRNA expression (Fig. 1F), (5) increased transcription of the tumor suppressor $p16^{INK4a}$ (Fig. 1F), and increased secretion of the pro-inflammatory cytokine IL-6 (Fig. 1G). Notably, siUBE2E3 cells secreted levels of IL-6 that were 5-fold greater than control siCON cells, whereas Etop treatment led to a 50-fold increase in IL-6 secretion (Fig. 1G). We also found that both siUBE2E3 and Etop treatment increased the forward (FSC) and side scatter (SSC) profiles of RPE-1 cells (Fig. 1H), a feature consistent with

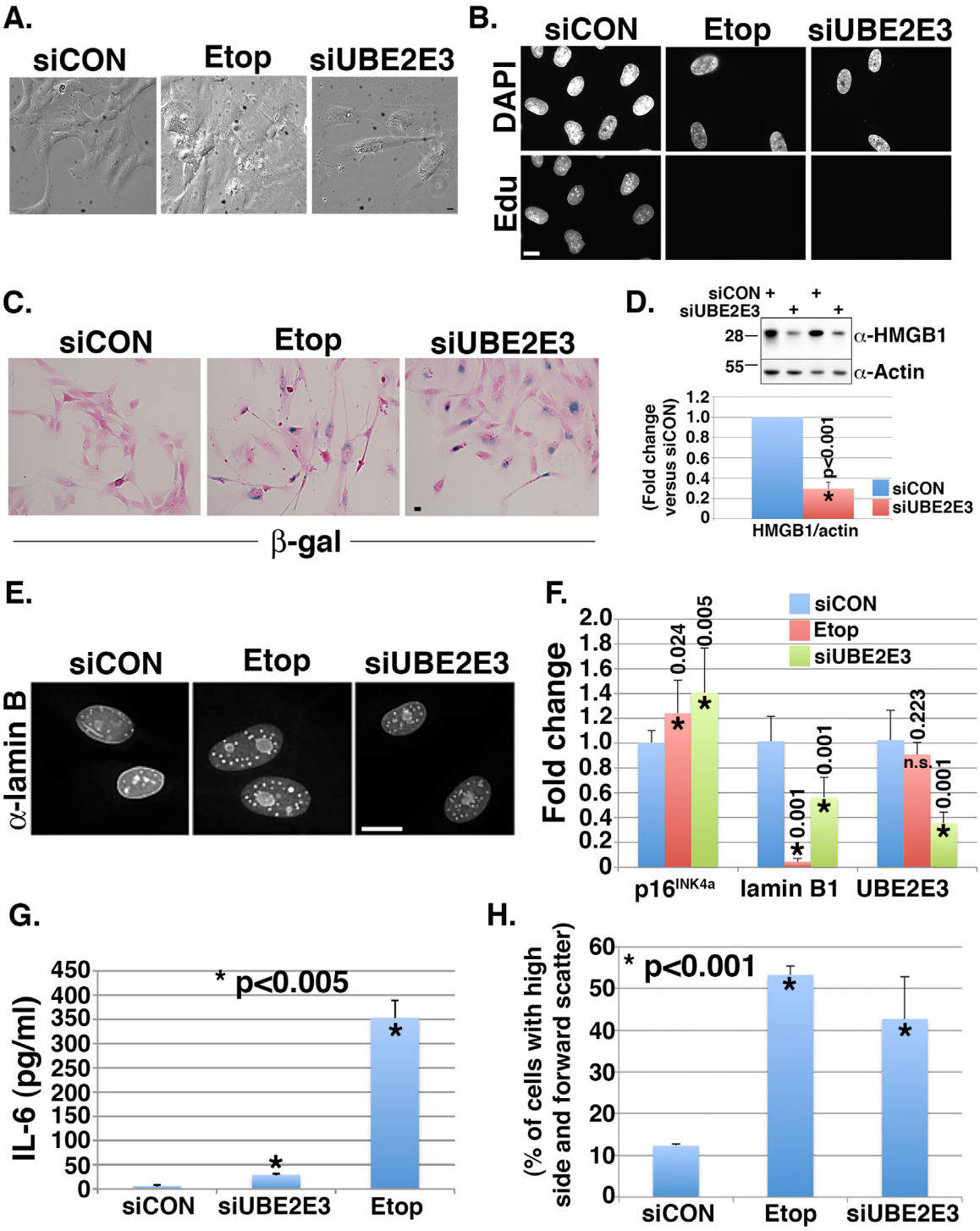

Fig. 1. Depletion of UBE2E3 induces cellular senescence. (A) Phase-contrast images of representative RPE-1 cells transfected with siCON or siUBE2E3 or treated with etoposide (Etop) and imaged 6 days post-siRNA. **(B)** Same experimental conditions as (A). Cells were labeled with Edu, a marker of proliferating cells, and nuclei were counterstained with DAPI. **(C)** RPE-1 cells were treated as indicated, fixed, and processed to detect the expression of lysosomal [pH6] β-gal (blue staining) and counterstained with eosin (pink). **(D)** Representative western blot of intracellular HMGB1 expression detected in lysates from two independent experiments. Migration of molecular weight markers is shown on the left. The graph is compiled from 6 independent experiments and actin expression was used to normalize all samples. **(E)** RPE-1 cells were treated as indicated, fixed, and processed for anti-lamin B immunolabeling. **(F)** Graph of fold change over siCON (blue bars) of mRNA levels of $p16^{INK4a}$, lamin B1, and UBE2E3. **(G)** Graph of IL-6 secreted into the media from 400,000 cells over a 24 h period as a function of the indicated treatments. **(H)** Graph showing % of cells with high forward and side scatter by FACS as a function of the indicated treatments. Graphs in (D), (F), (G), and (H) were each compiled from ≥ 3 independent experiments and asterisks denote statistical significance by one-way ANOVA compared to siCON cells; n.s. indicates no significance. Size bars in (A-C, E) represent 10 μm.

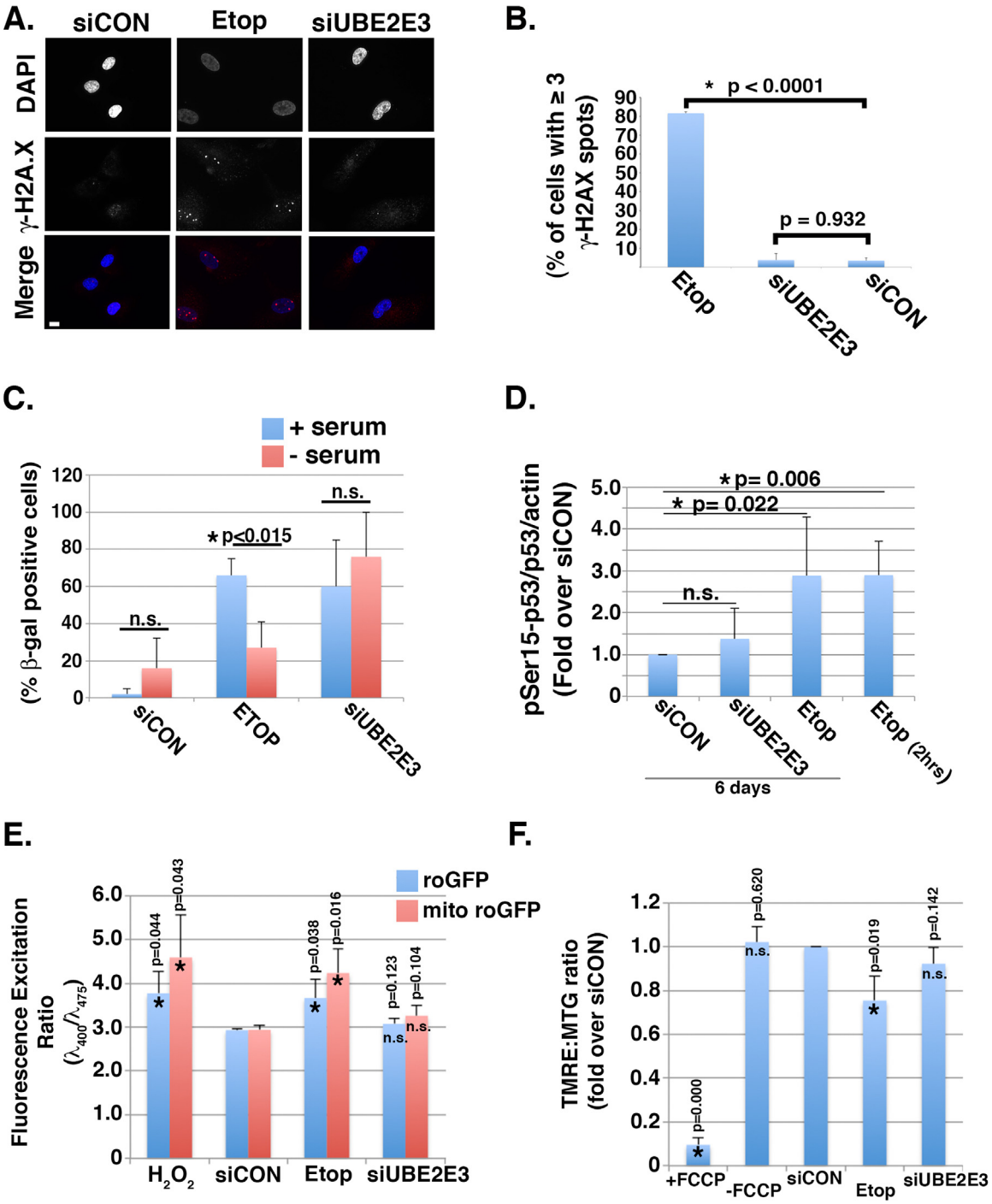

Fig. 2. Loss of UBE2E3 does not induce a DNA damage response. (A) siRNA-transfected or Etop-treated RPE-1 cells were fixed and immunolabeled with an antibody against γ-H2A.X, a marker of DNA double strand breaks, and DNA was counterstained with DAPI. Bottom panels show merged images. Size bar represents 10 μm. **(B)** Graph showing the percent of cells with 3 or more γ-H2A.X-positive spots in each nucleus as a function of treatment. **(C)** Graph showing the percent of cells stained positive for the expression of SA-β-gal as a function of being incubated with or without serum. **(D)** Graph showing quantifications from western blots of lysates derived from the indicated treatments. Lysates were resolved by SDS-PAGE and western blots done with antibodies against phospho-Ser15 p53, total p53, and actin. Values are expressed as fold change relative to the levels of each protein in siCON. Data compiled from 5 independent experiments. **(E)** Graph of FACS data demonstrating that UBE2E3 depletion does not cause intracellular redox stress. RPE-1 cells stably expressing the redox sensors roGFP- or mito-roGFP were treated as indicated and analyzed at excitation wavelengths of 405 nm and 488 nm and an emission wavelength of 525–530 nm. Values are normalized to siCON-transfected cells (i.e. fold over control) for each cell line. **(F)** Graph of the ratio of TMRE uptake to MTG uptake to assess the impact of each treatment on mitochondrial membrane potential. Values and statistics calculated as fold change compared to siCON, the value of which was set at 1.0. TMRE uptake by mitochondria is dependent upon an intact membrane potential whereas MTG labels mitochondria irrespective of membrane potential thereby allowing for normalization of mitochondrial mass between samples. FCCP dissipation of mitochondrial membrane potential demonstrates the sensitivity of the assay. Graphs in (B-F) were each compiled from ≥ 3 independent experiments and statistical significance was determined by one-way ANOVA compared to siCON cells. Asterisks denote statistical significance and 'n.s.' denotes not significant.

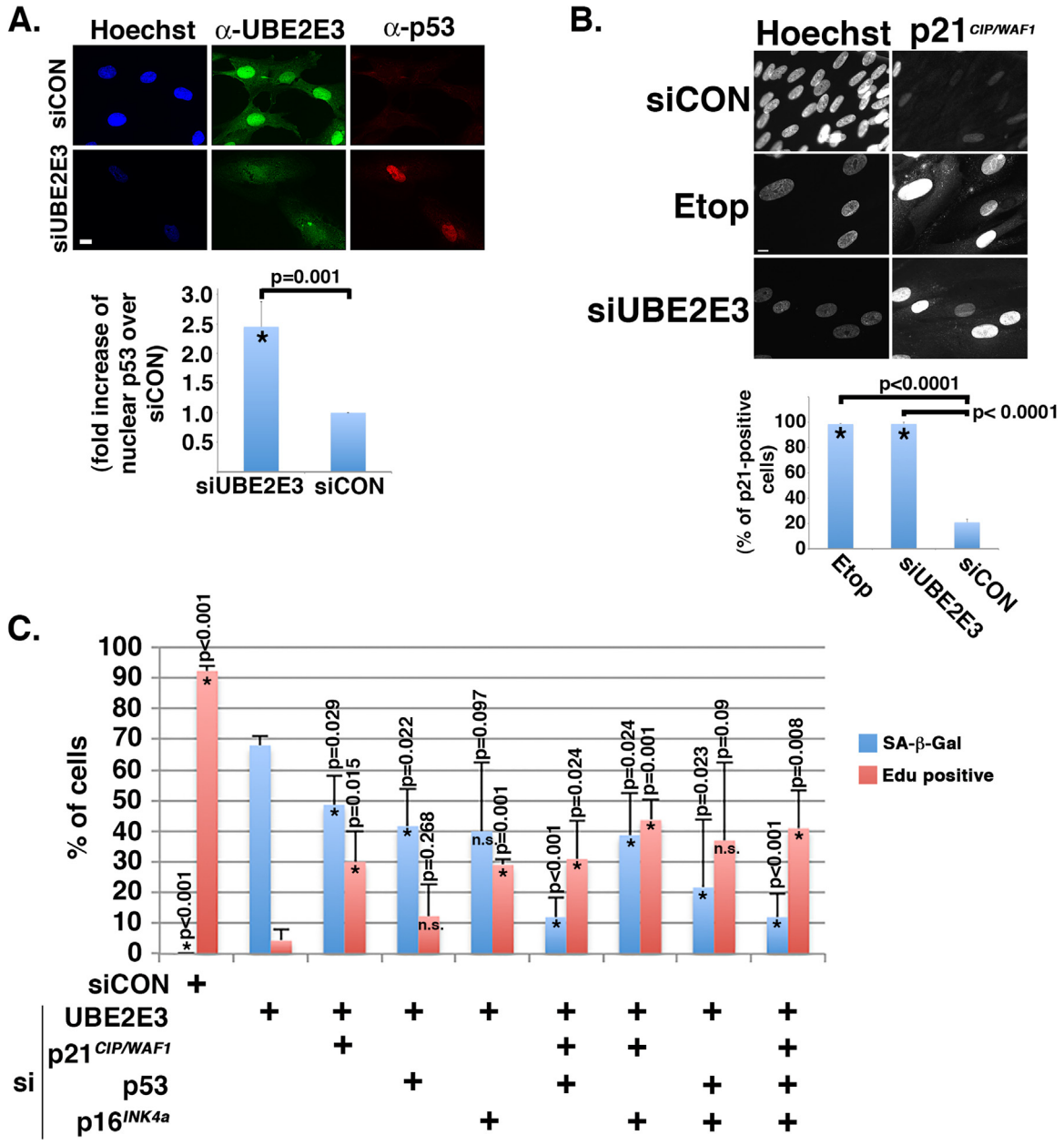

Fig. 3. Loss of UBE2E3 activates the p53 pathway. (A) Representative photomicrographs of control and siUBE2E3 cells fixed and labeled with antibodies against UBE2E3 (green) and p53 (red). Nuclei are counterstained with Hoechst (blue). Notably, the uptake of DNA counterstains by siUBE2E3 nuclei is reduced. Graph of fold increase of *nuclear* p53 labeling as a function of siRNA treatment. Levels of nuclear p53 in siCON set at 1.0. **(B)** Representative photomicrographs of siCON, Etop-treated, and siUBE2E3 cells fixed and labeled with an antibody against $p21^{CIP1/WAF1}$. Nuclei counterstained with Hoechst. Graph of percent of cells expressing nuclear $p21^{CIP1/WAF1}$ as a function of treatment. Asterisks in (A) and (B) indicate statistical significance by one-way ANOVA as compared to siCON. Data for each graph pooled from 3 independent experiments. **(C)** Graph compiled from three independent rescue experiments measuring the percent of cells expressing SA-β-gal (blue bars) or incorporating Edu (red bars) as a function of the indicated siRNA treatments. Asterisks indicate statistical significance by one-way ANOVA as compared to siUBE2E3 for either SA-β-Gal or Edu and 'n.s.' indicates not significant.

cellular senescence (e.g., [11]). Likewise, both siUBE2E3 cells and Etop-treated cells incorporated less of the DNA counterstains, DAPI (Fig. 2A, top panels) and Hoechst (see below, Fig. 3A-B) [51].

A major route to senescence is caused by the DNA damage response (DDR) pathway [25,44]. We therefore next tested if UBE2E3 depletion induces a DDR. 6-days post siUBE2E3 addition, cells were fixed and immunolabeled to detect phospho-γH2A.X foci, an established marker of double-stranded DNA breaks and a hallmark of DDR [39]. phospho-γH2A.X foci were observed in only a small fraction of siUBE2E3 cells and the number and frequency of these foci was comparable to siCON cells (Fig. 2A and B). In contrast, greater than 80% of Etop-treated cells contained 3 or more phospho-γH2A.X foci per cell. Consistent with the lack of γ-H2A.X-positive nuclei, we found that the proliferative burst required for the onset of DDR-induced senescence was not necessary for siUBE2E3-mediated expression of SA-β-gal; it did however greatly amplify the percent of Etop-treated cells that express SA-β-gal expression (Fig. 2C). Lysates from siUBE2E3 cells also did not contain elevated phosphorylation of p53 on Ser15 (Fig. 2D), an additional marker of the DDR [41]. This elevation of phospho-Ser15-p53 is induced rapidly by Etop (e.g., 2 h after Etop addition) and persists for at least 6 days (Fig. 2D).

As excessive reactive oxygen species (ROS) production by mitochondria can damage DNA and induce senescence [46] and siUBE2E3 cells have a disrupted mitochondrial distribution [34], we tested

whether depletion of UBE2E3 causes oxidative stress in either the cytoplasm or within the mitochondrial matrix. Using our established assay [30], intracellular redox stress was measured in RPE-1 cells stably expressing cytosolic or mitochondria-localized, redox-responsive GFP (roGFP and mito-roGFP, respectively). roGFP is an enhanced variant with two redox-sensing cysteines in the beta barrel of the GFP. The redox status of these cysteines regulates the excitation profile of the roGFP; 400 nm excitation increases if the cysteines are oxidized and 475 nm excitation is favored when they are reduced. Both states emit at 510 nm. This GFP-based sensor enables free radical production and cellular redox status to be indirectly assessed [15]. The sensitivity of this assay was confirmed by analyzing cells treated acutely with hydrogen peroxide. Depletion of UBE2E3 did not induce a redox stress in either cellular compartment whereas Etop caused both a cytosolic and a mitochondrial redox stress (Fig. 2E).

Consistent with these findings, knockdown of UBE2E3 also did not cause a loss of mitochondrial membrane potential, as assessed by co-labeling mitochondria with tetramethylrhodamine ethyl ester (TMRE) and MitoTracker Green™ (MTG) and performing flow cytometry to calculate the median TMRE/MTG ratio compared to siCON cells, as we reported previously [30]. This approach is predicated on TMRE selectively labeling mitochondria with an intact membrane potential whereas MTG labels cytosolic mitochondria irrespective of membrane potential. The sensitivity of this assay was demonstrated by treating cells with carbonyl cyanide-4-(trifluoromethoxy)phenylhydrazone (FCCP), which depolarizes the mitochondrial membrane potential, thereby decreasing the TMRE:MTG ratio 10-fold (Fig. 2F, compare '+FCCP' to '-FCCP'). Consistent with the roGFP data, siUBE2E3 did not alter the TMRE: MTG ratio whereas Etop decreased the ratio, all compared to siCON (Fig. 2F). These findings indicate that siUBE2E3 does not cause senescence via increased ROS leakage or dissipating the mitochondrial membrane potential, both of which can result in a DDR [46,48]. Conversely, Etop treatment resulted in both a redox stress and a compromised mitochondrial membrane potential, in alignment with the previously reported phenomenon linking DDR to mitochondrial dysfunction via increased ROS-mediated, genomic DNA damage [31]. Collectively, the data described in Fig. 2 support that loss of UBE2E3 is not promoting senescence via DNA damage and an ensuing DDR.

We next examined siUBE2E3 cells for changes in the levels of nuclear p53, which increases in human fibroblasts that become senescent in the absence of a DDR [3]. α-p53 immunofluorescence showed a 2.5-fold increase in nuclear p53 levels in siUBE2E3 cells compared to controls (Fig. 3A). Moreover, this increased nuclear p53 corresponded to an increase in transcriptional activity as shown by the elevated expression of a known target gene, the cell cycle inhibitor and senescence marker, $p21^{CIP1/WAF1}$ (Fig. 3B). Elevation of $p21^{CIP1/WAF1}$ was modest at 3 days post-siRNA (data not shown) but robust by 6 days (Fig. 3B). We further demonstrated the importance of p53, $p21^{CIP1/WAF1}$, and $p16^{INK4a}$ to siUBE2E3-induced senescence through co-knockdown rescue experiments. Using a combination of co-knockdowns and measuring both SA-β-Gal expression as well as Edu incorporation in the same cells, 4 days after siRNA administration, we found that silencing the expression of either p53 or $p21^{CIP1/WAF1}$ mitigated the siUBE2E3-induced SA-β-gal expression whereas silencing either $p21^{CIP1/WAF1}$ or $p16^{INK4a}$ mitigated the cell cycle exit (Fig. 3C). Further, combinatorial silencing of $p21^{CIP1/WAF1}$ and either p53 or $p16^{INK4a}$ rescued both markers (Fig. 3C). Together, these data highlight the relevance of p53 nuclear activation to siUBE2E3-mediated senescence, mirroring what has been reported regarding p53-dependent senescence [3]. The knockdown efficiencies of p53 and $p21^{CIP1/WAF1}$ were validated by western blotting and that of $p16^{INK4a}$ by qPCR (data not shown).

We next investigated a recently-discovered, alternative pathway of senescence originating from mitochondrial dysfunction [48]. This pathway is termed mitochondrial dysfunction associated senescence (MiDAS), and it is distinguished from the DDR in numerous ways, most notably for having a distinct senescence-associated secretory phenotype (SASP) [48]. Our rationale for considering MiDAS stemmed from observations linking siUBE2E3 cells to disrupted mitochondrial homeostasis. We previously reported that depletion of UBE2E3 causes a collapse of the mitochondrial network from its typically reticular distribution to a perinuclear tangle [34]. Second, depletion of the enzyme dramatically increased the susceptibility of RPE cells to apoptosis in response to the mitochondrial poison FCCP, as well as to chloroquine, an inhibitor of lysosomal-mediated degradation (Fig. 4A). And third, siUBE2E3 cells contain 30% more mitochondria than control cells as measured by MitoTracker Green™ (MTG) uptake and 60% more mitochondria as measured by mito-tdTomato and quantified by flow cytometry (Fig. 4B). For these experiments, Mito-tdTomato expressing RPE-1 cells were labeled with MTG. Mito-tdTomato is acid resistant and therefore labels mitochondria in acidic vesicles (e.g., lysosomes) as well as those not in acidic vesicles whereas MTG only labels mitochondria that are in the cytoplasm and not enclosed inside acidic vesicles. Thus, this assay measures both total mitochondrial content (mito-tdTomato) as well as the levels of cytosolic mitochondria (MTG). siUBE2E3 cells had increases in both cytosolic mitochondria as well as mitochondria in acidic vesicles, presumably destined for lysosomal degradation. Increases in mitochondrial mass are commonly reported in senescent cells [9], and consistent with this, Etop treatment also increased mitochondrial content (Fig. 4B).

To determine if siUBE2E3 cells have the distinguishing SASP profile characteristic of MiDAS, we analyzed a panel of SASP factors by qPCR. Specifically, we measured the mRNA levels of IL-1β, IL-6, IL-8, IL-10, CXCL1, and CXCL2. Surprisingly, UBE2E3 depletion only increased IL-1β whereas Etop led to an increase in all of the factors except IL-10. In fact, the increase in IL-1β in siUBE2E3 cells was markedly suppressed as compared to Etop-treated cells (Fig. 4C and D). These data indicate that loss of UBE2E3 induces senescence characterized by a distinct SASP and is distinguished from MiDAS by lacking a robust IL-10 up-regulation.

Although knockdown of UBE2E3 did not detectably damage mitochondrial integrity (Fig. 2E and F), the increased sensitivity of siUBE2E3 cells to the mitochondrial poison, FCCP (Fig. 4A), along with the increase in vesicle-associated mitochondrial mass (Fig. 4B), prompted us to analyze mitophagy in siUBE2E3 cells. Mitophagy is a specialized autophagy pathway that triages irreparably damaged mitochondria to lysosomes for degradation [16]. These experiments used an assay based on the mt-mKeima reporter protein [24,30], a coral-derived, acid-stable, red fluorescent protein with a mitochondria-targeting sequence. This reporter exhibits pH-dependent excitation properties and is resistant to lysosomal proteases [19]. Mt-mKeima excites at 448 nm in neutral pH and at 561 nm in an acidic environment, and these two populations can be distinguished and quantified by flow cytometry. The 448 nm population represents healthy, cytosolic mitochondria, and the 561 nm population represents mitochondria within lysosomes en route for degradation [19,42]. The sensitivity of this assay is demonstrated by an increase in the lysosomal mt-mKeima signal upon the induction of mitophagy with FCCP and a corresponding decrease in cytosolic mitochondria (Fig. 5A). Notably, siCON control cells display minimal mitophagic flux. siUBE2E3 cells and Etop-treated cells have dramatic increases in lysosome-associated mitochondria (Fig. 5A). Furthermore, siUBE2E3 (and Etop-treated) cells correspondingly contain an increase in overall lysosomal mass as shown by increased uptake of the lysosome-specific dye, LysoTracker™(LTR; Fig. 5B and C), and independently, by increased uptake of the lysosomal marker, acridine orange (Fig. 5D). The LTR flow cytometry assay uses forward scatter to normalize for cell size [7] and the acridine orange flow cytometry assay uses autofluorescence in the green channel to normalize for cell size [45].

The above data indicated that autophagic flux is altered in cells depleted of UBE2E3. To assess autophagic flux, we generated an RPE-1 cell line stably expressing GFP-tagged LC3 (GFP-LC3), a reliable proxy for monitoring autophagy [14,40]. Two populations of GFP-LC3 are readily observed, a diffuse population not engaged with the autophagic

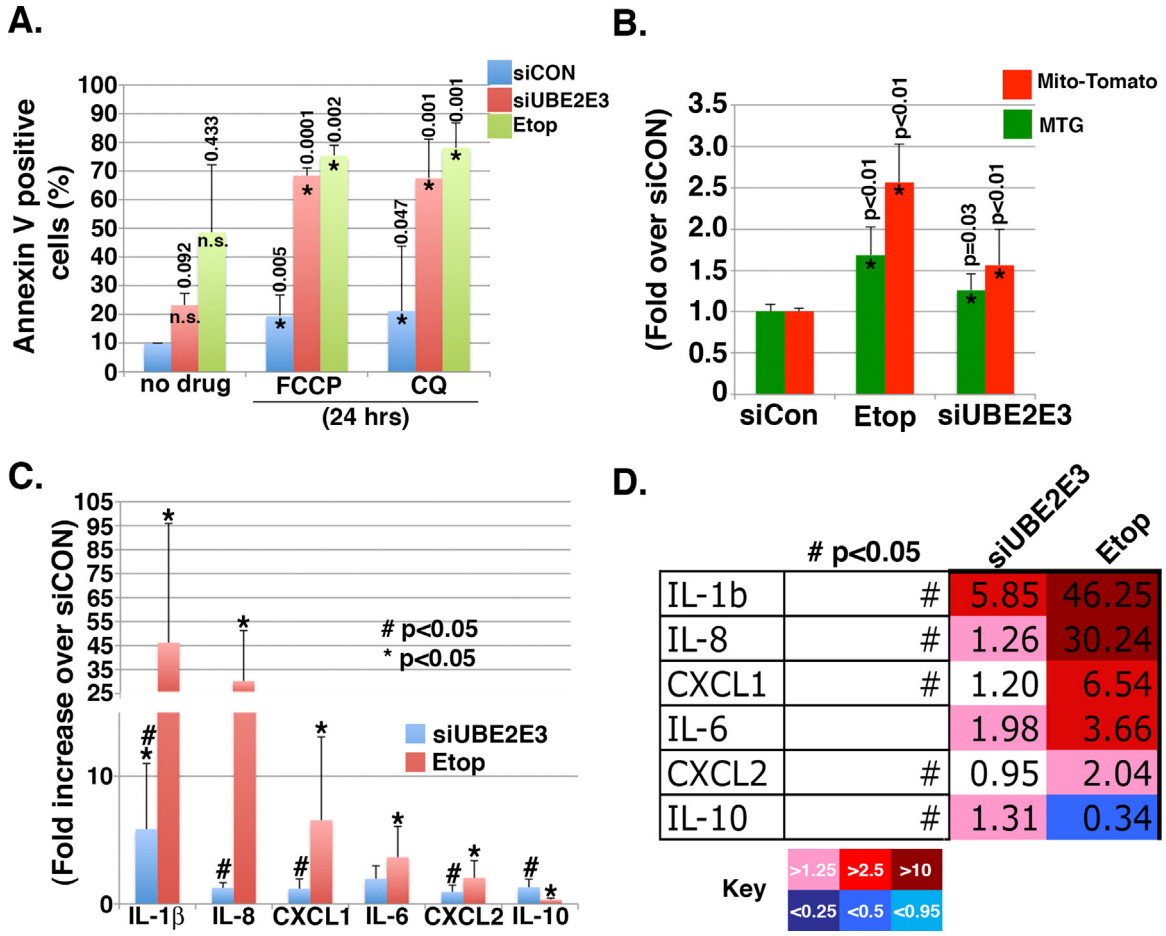

Fig. 4. UBE2E3-depleted cells have increased mitochondrial mass and a distinct SASP. (A) UBE2E3 depleted cells have an increased susceptibility to cell death following treatment with the mitochondrial poison, FCCP, or the lysosomal deacidifier, chloroquine (CQ). Graph of data compiled from FACS analyses detecting Annexin V expression in unpermeabilized cells. p values were calculated by comparison to siCON + no drug. Asterisks denote statistical significance. **(B)** FACS analysis measuring Mito-tomato expression (red bars) and MitoTracker Green (MTG; green bars) uptake. Mito-tomato derived-fluorescence represents the entire cellular mitochondrial mass (free mitochondria plus mitochondria enclosed in autophagic vesicles) whereas MTG-derived fluorescence represents only the population of mitochondria that are *not* inside vesicles. Asterisks denote statistical significance compared to respective siCON cells. **(C)** qPCR analysis of the indicated SASP factors in cells treated with siCON, siUBE2E3 (pale blue bars), or Etop (red bars). siCON values for each factor have been set at 1.0 and are not shown but rather being used a reference point. Asterisks denote statistical significance compared to siCON whereas '#' denotes statistical significance in comparison to Etop sample. **(D)** Heat map of data presented in (C) with a key defining the color scale used. Pink, red, and crimson indicate values > siCON and light, medium, and dark blue indicate values < siCON. p values throughout this figure were determined by one-way ANOVA with samples being compared to siCON control cells, unless otherwise noted. Each graph compiled from 3 independent experiments. Asterisks in (A) and (B) indicate statistical significance and 'n.s.' denotes not significant.

machinery and a second population that is punctiform in appearance due to its recruitment to early autophagic vesicles (Fig. 5E, panel a). siUBE2E3 cells have increased basal levels of vesicle-associated GFP-LC3 and a corresponding decrease in diffuse, cytosolic GFP-LC3 (Fig. 5E, panel d and Fig. 5F). When cells were challenged with chloroquine (CQ), a reagent that raises lysosomal pH and thereby blocks the catabolic step of autophagy [20], the increased basal autophagic flux in siUBE2E3 cells was amplified (Fig. 5E, panel *d* versus *e*). Acute treatment with the mitophagy inducer FCCP led to elevated GFP-LC3 associated with vesicles in siCON cells (Fig. 5E, panel *a* versus *c*) as well as siUBE2E3 cells, indicating that siUBE2E3 cells retain the capacity to further induce the autophagy machinery (Fig. 5E, compare panels *d* versus *f*). This induction of autophagy was confirmed quantitatively by FACS analysis of vesicle-associated GFP-LC3 (Fig. 5F). In this assay, we specifically quantified vesicle-associated GFP-LC3 by FACS analysis after detergent-permeabilization to leak out the cytosolic GFP-LC3. Interestingly, vesicle-associated GFP-LC3 and LTR-stained lysosomes in siUBE2E3 cells were typically in a perinuclear pattern resembling a wreath (Fig. 5C, panel b and Fig. 5E, panels d-f).

To further interrogate the impact of UBE2E3 depletion on autophagy, we induced autophagy in GFP-LC3 expressing RPE-1 cells by starvation via the deprivation of both amino acids and growth factors (i.e., -aa/-gfs) for 2 h. As expected, siCON cells responded to this nutrient deprivation by increasing vesicle-associated GFP-LC3 and decreasing diffuse, cytosolic GFP-LC3 (Fig. 6A, panel a versus b). Interestingly, cells depleted of UBE2E3 responded to nutrient deprivation by resolving their perinuclear, basal accumulation of punctiform GFP-LC3 (Fig. 6A, panel c versus d). Quantification of vesicle-associated GFP-LC3 by FACS analysis showed that: (a) basal autophagosome-associated GFP-LC3 is 50% higher in siUBE2E3 cells compared to siCON cells (in complete media; Fig. 6B, compare blue bars), (b) as expected, acute starvation induced a nearly 2-fold increase of autophagosome GFP-LC3 in siCON cells, and (c) surprisingly, although starvation dramatically decreases the perinuclear accumulation of GFP-LC3-positive vesicles in siUBE2E3 cells (Fig. 6A, panel c versus d), the total levels of this population of the reporter do not decrease significantly but also do not increase upon starvation, as observed in siCON cells (Fig. 6B). Collectively, we interpret these data to indicate that siUBE2E3 cells have an increased autophagic load and flux that congests the autophagy system under basal conditions, but upon further induction of the autophagy

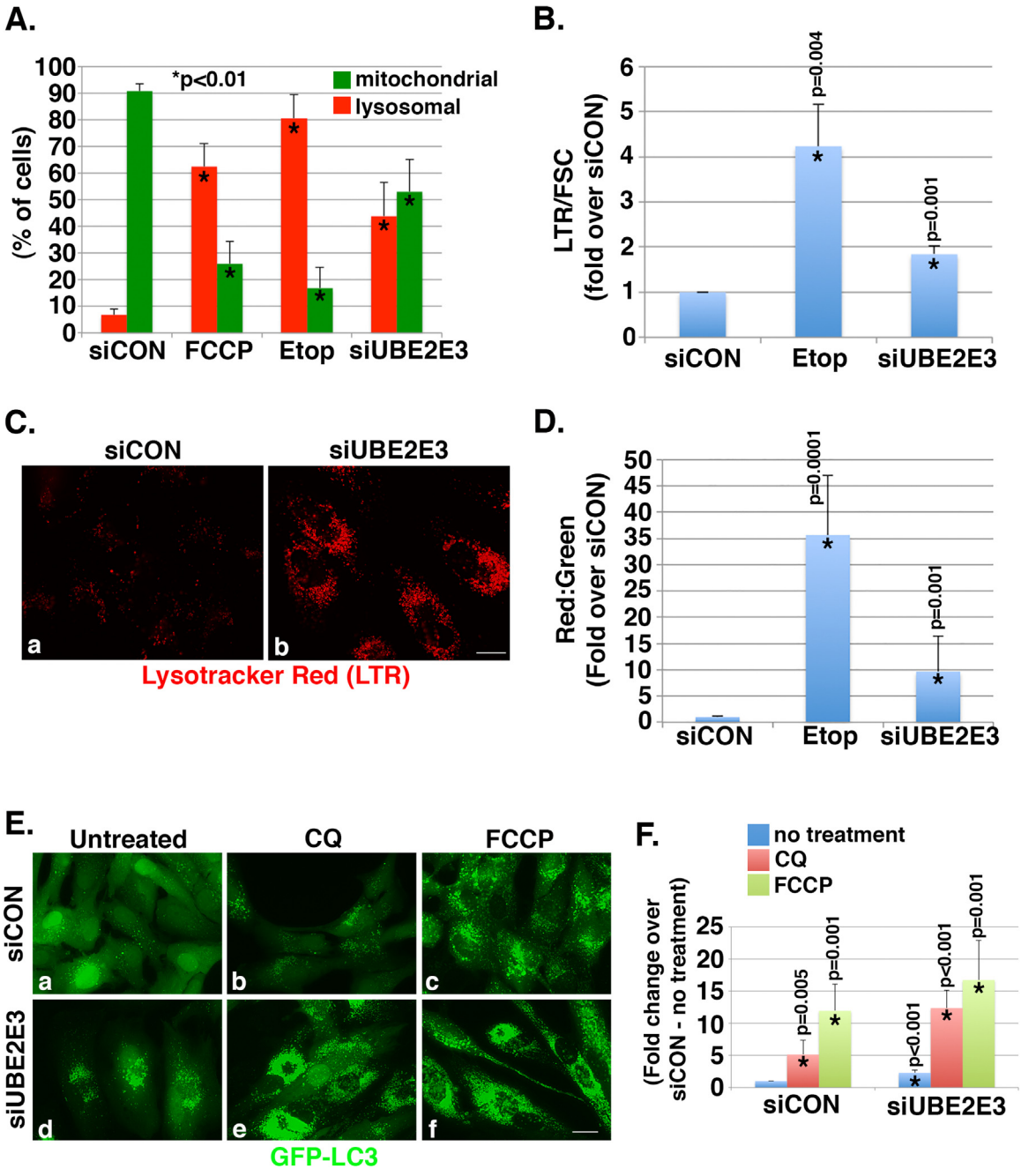

Fig. 5. UBE2E3 depletion increases mitochondrial and lysosomal content and autophagic flux. (A) mt-mKeima-expressing RPE-1 cells were treated as indicated and analyzed by FACS analysis to measure excitation profiles of the mt-mKeima at 448 nm (neutral pH) and at 561 nm (acidic pH). This assay defines mitochondria as being in the cytoplasm (green bars) versus being within an acidic compartment along the autophagy-lysosomal pathway (red bars). FCCP treatment serves as a positive control to show that damaging the mitochondria shifts the excitation profile in favor of mitophagy. **(B)** Cells were treated with siCON, Etop, or siUBE2E3 and 6 days later incubated with LysoTracker Red (LTR) prior to being harvested for FACS. Forward scatter (FSC) was used to normalize for cell size. **(C)** Representative photomicrographs of RPE-1 cells treated with the indicated siRNAs and labeled with LTR. **(D)** Graph of acridine orange uptake by lysosomes (red) as a function of cell size (green; autofluorescence) for the indicated treatments with the ratio of red: green plotted on the y-axis. Data expressed as fold change over siCON. **(E)** Representative photomicrographs of GFP-LC3 expressing RPE-1 cells incubated with the indicated siRNAs and 3 days later treated acutely with chloroquine (CQ) or FCCP. Untreated controls shown for comparison. **(F)** Graph of FACS analysis measuring vesicle-associated GFP-LC3 following detergent-permeabilization of cells to leak out cytosolic GFP-LC3. Data graphed as fold increase over siCON + "no treatment". Cells were challenged with either chloroquine (CQ, red bars) or FCCP (light green bars) for 4 h prior to harvesting. For (A), (B), (D), and (F), each graph was compiled from 3 independent experiments and statistical significance was calculated by comparison to siCON, using one-way ANOVA. Asterisks denote statistical significance. Size bars in (C) and (E) are 10 μm.

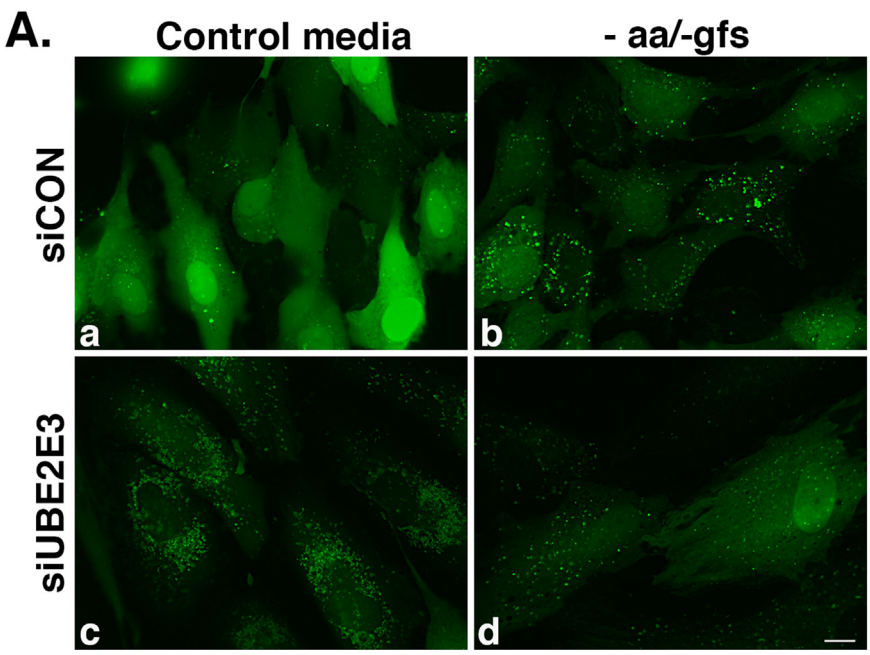

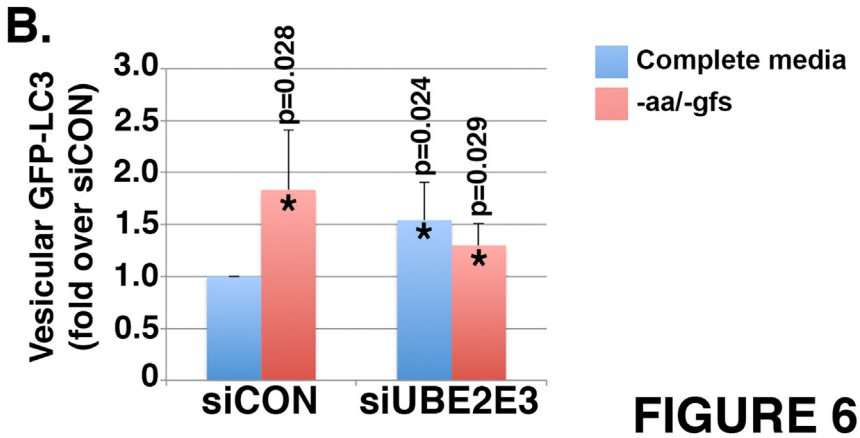

Fig. 6. Nutrient deprivation restores autophagic flux in siUBE2E3 cells. (A) Representative photomicrographs of GFP-LC3 expressing RPE-1 cells transfected with the indicated siRNAs and incubated in either complete media (control media) or starved of amino acids (- aa) and growth factors (i.e., - gfs) for 2 h prior to being processed for microscopy. Size bar in (A) is 10 μm. **(B)** Graph of vesicle-associated GFP-LC3 quantified by FACS analysis after detergent extraction of cytosolic GFP-LC3. Data expressed as fold over siCON in complete media with graph compiled from 3 independent experiments. p values determined by one-way ANOVA with all samples being compared to siCON control cells in complete media. Asterisks denote statistical significance.

FIGURE 6

machinery (e.g., via nutrient starvation), this back-up can be at least partially resolved.

4. Discussion

The studies of this report detail the cellular senescence phenotype induced by depletion of the metazoan ubiquitin conjugating enzyme UBE2E3. This enzyme constitutively shuttles in and out of the nucleus [36,37], interacts with multiple E3 ligase partners [2,28,35,36], is largely restricted to transferring mono-Ub to its cognate substrates [28], and regulates the distribution of the mitochondrial network within the cell [34]. Efforts to elucidate the cellular functions of this enzyme have revealed that it is required for cell proliferation [32] and for the proper localization and activation of the anti-stress transcription factor Nrf2 [34]. Notably, our efforts to generate a global knockout of the enzyme in mice demonstrated that loss of UBE2E3 is embryonic lethal (unpublished data). One explanation for this embryonic lethality may be that cells lacking the enzyme irreversibly exit the cell cycle and become senescent. Moreover, of potential relevance to cellular senescence in the context of neurodegeneration, we previously reported that the expression levels of UbcM2 (the identical version of human UBE2E3 expressed by mice) decrease as a function of age in five substructures of the brain: the cerebellar granule cell layer, the primary motor cortex, the olfactory nucleus, the superior colliculus, and the secondary visual cortex [23].

Characterization of siUBE2E3-mediated senescence has revealed a senescence signature that does not phenocopy DDR or MiDAS but rather parallels numerous aspects of PTEN-loss induced cellular senescence (PICS) [1] and AKT-induced cellular senescence [3]. Similar to the described PICS and AKT pathways, siUBE2E3-mediated senescence occurs independently of overt genomic damage and does not require the brief proliferative burst that precedes DDR and OIS. All three pathways also involve up-regulation and activation of p53 and its down-stream target, $p21^{CIP1/WAF1}$ (Fig. 3), modest increases in the cell cycle inhibitor $p16^{INK4a}$ (Fig. 1F), and a critical role for mTOR signaling (data not shown). Interestingly, PTEN and UBE2E3 share a common nuclear import receptor, called importin-11 [36,6], although whether and how this transport receptor links the two enzymes to senescence remains to be determined.

A second intriguing aspect of siUBE2E3-mediated senescence is the distinct SASP (Fig. 4C-D). A mitigated SASP has been demonstrated for MiDAS, a specialized type of senescence derived from dysfunctional mitochondria [48]. However, MiDAS induces a robust up-regulation of several factors including IL-10 but notably has an absence of the IL-1β arm [48]. In contrast, siUBE2E3-induced senescence caused a very modest increase in IL-10 mRNA expression but a nearly 6-fold increase in IL-1β mRNA. This profile indicates that siUBE2E3 cells combine aspects of several different senescence pathways, which may reflect the multiple E3 ligases and range of functions linked to the enzyme [28,33,34].

We favor a model in which siUBE2E3 cells become senescent due to a disruption in the maintenance of the mitochondrial network. The basis for this model is that knockdown of the enzyme alters multiple features of mitochondrial homeostasis, including distribution [34], susceptibility to poisons (Fig. 4A), mass (Fig. 4B), and increased basal autophagy/mitophagy (Fig. 5A). In addition, UBE2E3 specifically interacts with Mulan, an E3 ligase that resides in the mitochondrial outer membrane and regulates mitochondrial dynamics and function [2,26,38,8]. Mulan has the distinguishing feature that it can target substrates with Ub or SUMO, depending on the E2 it binds. As UBE2E3 conjugates Ub [10,28], we anticipate that the pair modifies cognate substrates with Ub to modulate mitophagic flux. Consistent with this idea, the Zervos lab demonstrated that a fusion of UBE2E3 and the cytoplasmic tail of Mulan bind specifically and selectively to GABAA receptor-associated protein (GABARAP), an ATG8 ortholog required for autophagosome-lysosome fusion, a key late step in mitophagy [29]. This interaction is highly specific as GABARAP did not interact with the tail of Mulan alone or with the tail of Mulan fused to UBE2E2, an enzyme that is > 90% identical to UBE2E3 [2]. One implication predicted by our findings is that UBE2E3 and Mulan restrict GABARAP function, consistent with increased autophagic flux upon UBE2E3 depletion (Figs. 5 and 6). Future work will establish whether and how disrupting this UBE2E3-Mulan-GABARAP axis impacts mitochondrial homeostasis and drives cellular senescence.

Acknowledgements

This work was supported in part by The National Institutes of Health Grant (R01EY024944 to S.M.P.), an Oklahoma Center for the Advancement of Science and Technology Grant (HR16-068 to S.M.P.), and with monies from the Presbyterian Health Foundation (to S.M.P.). None of the funding agencies were directly involved in the design of experiments, nor the collection or interpretation of data. We are very grateful to past and present members of the Plafker laboratory for insightful discussions.

The authors have no competing interests or conflicts to declare.

References

[1] A. Alimonti, C. Nardella, Z. Chen, J.G. Clohessy, A. Carracedo, L.C. Trotman, K. Cheng, S. Varmeh, S.C. Kozma, G. Thomas, et al., A novel type of cellular senescence that can be enhanced in mouse models and human tumor xenografts to suppress prostate tumorigenesis, J. Clin. Investig. 120 (2010) 681–693.

[2] C.T. Ambivero, L. Cilenti, S. Main, A.S. Zervos, Mulan E3 ubiquitin ligase interacts with multiple E2 conjugating enzymes and participates in mitophagy by recruiting GABARAP, Cell. Signal. 26 (2014) 2921–2929.

[3] M.V. Astle, K.M. Hannan, P.Y. Ng, R.S. Lee, A.J. George, A.K. Hsu, Y. Haupt, R.D. Hannan, R.B. Pearson, AKT induces senescence in human cells via mTORC1 and p53 in the absence of DNA damage: implications for targeting mTOR during malignancy, Oncogene 31 (2012) 1949–1962.

[4] D.J. Baker, R.C. Petersen, Cellular senescence in brain aging and neurodegenerative diseases: evidence and perspectives, J. Clin. Investig. 128 (4) (2018) 1208–1216.

[5] J. Campisi, Aging, cellular senescence, and cancer, Annu. Rev. Physiol. 75 (2013) 685–705.

[6] M. Chen, D.G. Nowak, N. Narula, B. Robinson, K. Watrud, A. Ambrico, T.M. Herzka, M.E. Zeeman, M. Minderer, W. Zheng, et al., The nuclear transport receptor Importin-11 is a tumor suppressor that maintains PTEN protein, J. Cell Biol. 216 (2017) 641–656.

[7] S. Chikte, N. Panchal, G. Warnes, Use of LysoTracker dyes: a flow cytometric study of autophagy, Cytom. Part A: J. Int. Soc. Anal. Cytol. 85 (2014) 169–178.

[8] L. Cilenti, C.T. Ambivero, N. Ward, E.S. Alnemri, D. Germain, A.S. Zervos, Inactivation of Omi/HtrA2 protease leads to the deregulation of mitochondrial Mulan E3 ubiquitin ligase and increased mitophagy, Biochim. Biophys. Acta 1843 (2014) 1295–1307.

[9] C. Correia-Melo, F.D. Marques, R. Anderson, G. Hewitt, R. Hewitt, J. Cole, B.M. Carroll, S. Miwa, J. Birch, A. Merz, et al., Mitochondria are required for pro-ageing features of the senescent phenotype, EMBO J. 35 (2016) 724–742.

[10] Y. David, T. Ziv, A. Admon, A. Navon, The E2 ubiquitin-conjugating enzymes direct polyubiquitination to preferred lysines, J. Biol. Chem. 285 (2010) 8595–8604.

[11] E. Deruy, K. Gosselin, C. Vercamer, S. Martien, F. Bouali, C. Slomianny, J. Bertout, D. Bernard, A. Pourtier, C. Abbadie, MnSOD upregulation induces autophagic programmed cell death in senescent keratinocytes, PLoS One 5 (2010) e12712.

[12] I. Dikic, Proteasomal and autophagic degradation systems, Annu Rev. Biochem. 86 (2017) 193–224.

[13] K.E. Eng, M.D. Panas, G.B. Karlsson Hedestam, G.M. McInerney, A novel quantitative flow cytometry-based assay for autophagy, Autophagy 6 (2010) 634–641.

[14] C. Fung, R. Lock, S. Gao, E. Salas, J. Debnath, Induction of autophagy during extracellular matrix detachment promotes cell survival, Mol. Biol. Cell 19 (2008) 797–806.

[15] G.T. Hanson, R. Aggeler, D. Oglesbee, M. Cannon, R.A. Capaldi, R.Y. Tsien, S.J. Remington, Investigating mitochondrial redox potential with redox-sensitive green fluorescent protein indicators, J. Biol. Chem. 279 (2004) 13044–13053.

[16] J.W. Harper, A. Ordureau, J.M. Heo, Building and decoding ubiquitin chains for mitophagy, Nat. Rev. Mol. Cell Biol. 19 (2018) 93–108.

[17] A. Hernandez-Segura, J. Nehme, M. Demaria, Hallmarks of Cellular Senescence. Trends Cell Biol. Feb 21. pii: S0962-8924(18)30020-5, 2018.

[18] D. Jurk, C. Wang, S. Miwa, M. Maddick, V. Korolchuk, A. Tsolou, E.S. Gonos, C. Thrasivoulou, M.J. Saffrey, K. Cameron, et al., Postmitotic neurons develop a p21-dependent senescence-like phenotype driven by a DNA damage response, Aging Cell 11 (2012) 996–1004.

[19] H. Katayama, T. Kogure, N. Mizushima, T. Yoshimori, A. Miyawaki, A sensitive and quantitative technique for detecting autophagic events based on lysosomal delivery, Chem. Biol. 18 (2011) 1042–1052.

[20] D.J. Klionsky, F.C. Abdalla, H. Abeliovich, R.T. Abraham, A. Acevedo-Arozena, K. Adeli, L. Agholme, M. Agnello, P. Agostinis, J.A. Aguirre-Ghiso, et al., Guidelines for the use and interpretation of assays for monitoring autophagy, Autophagy 8 (2012) 445–544.

[21] D. Komander, M. Rape, The ubiquitin code, Annu. Rev. Biochem. 81 (2012) 203–229.

[22] N. Kubben, W. Zhang, L. Wang, T.C. Voss, J. Yang, J. Qu, G.H. Liu, T. Misteli, Repression of the antioxidant NRF2 pathway in premature aging, Cell 165 (2016) 1361–1374.

[23] C.M. Larabee, C. Georgescu, J.D. Wren, S.M. Plafker, Expression profiling of the ubiquitin conjugating enzyme UbcM2 in murine brain reveals modest age-dependent decreases in specific neurons, BMC Neurosci. 16 (2015) 76–86.

[24] M. Lazarou, D.A. Sliter, L.A. Kane, S.A. Sarraf, C. Wang, J.L. Burman, D.P. Sideris, A.I. Fogel, R.J. Youle, The ubiquitin kinase PINK1 recruits autophagy receptors to induce mitophagy, Nature 524 (2015) 309–314.

[25] O.V. Leontieva, M.V. Blagosklonny, DNA damaging agents and p53 do not cause senescence in quiescent cells, while consecutive re-activation of mTOR is associated with conversion to senescence, Aging 2 (2010) 924–935.

[26] W. Li, M.H. Bengtson, A. Ulbrich, A. Matsuda, V.A. Reddy, A. Orth, S.K. Chanda, S. Batalov, C.A. Joazeiro, Genome-wide and functional annotation of human E3 ubiquitin ligases identifies MULAN, a mitochondrial E3 that regulates the organelle's dynamics and signaling, PLoS One 3 (2008) e1487.

[27] T.G. McWilliams, M.M. Muqit, PINK1 and Parkin: emerging themes in mitochondrial homeostasis, Curr. Opin. Cell Biol. 45 (2017) 83–91.

[28] L. Nguyen, K.S. Plafker, A. Starnes, M. Cook, R.E. Klevit, S.M. Plafker, The ubiquitin-conjugating enzyme, UbcM2, is restricted to monoubiquitylation by a two-fold mechanism that involves backside residues of E2 and Lys48 of ubiquitin, Biochemistry 53 (2014) 4004–4014.

[29] T.N. Nguyen, B.S. Padman, J. Usher, V. Oorschot, G. Ramm, M. Lazarou, Atg8 family LC3/GABARAP proteins are crucial for autophagosome-lysosome fusion but not autophagosome formation during PINK1/Parkin mitophagy and starvation, J. Cell Biol. 215 (2016) 857–874.

[30] G.B. O'Mealey, K.S. Plafker, W.L. Berry, R. Janknecht, J.Y. Chan, S.M. Plafker, A PGAM5-KEAP1-Nrf2 complex is required for stress-induced mitochondrial retrograde trafficking, J. Cell Sci. 130 (20) (2017) 3467–3480.

[31] J.F. Passos, G. Nelson, C. Wang, T. Richter, C. Simillion, C.J. Proctor, S. Miwa, S. Olijslagers, J. Hallinan, A. Wipat, et al., Feedback between p21 and reactive oxygen production is necessary for cell senescence, Mol. Syst. Biol. 6 (2010) 347.

[32] K.S. Plafker, K.M. Farjo, A.F. Wiechmann, S.M. Plafker, The human ubiquitin conjugating enzyme, UBE2E3, is required for proliferation of retinal pigment epithelial cells, Investig Ophthalmol. Vis. Sci. 49 (12) (2008) 5611–5618.

[33] K.S. Plafker, L. Nguyen, M. Barneche, S. Mirza, D. Crawford, S.M. Plafker, The ubiquitin-conjugating enzyme UbcM2 can regulate the stability and activity of the antioxidant transcription factor Nrf2, J. Biol. Chem. 285 (2010) 23064–23074.

[34] K.S. Plafker, S.M. Plafker, The ubiquitin-conjugating enzyme UBE2E3 and its import receptor importin-11 regulate the localization and activity of the antioxidant transcription factor NRF2, Mol. Biol. Cell 26 (2015) 327–338.

[35] K.S. Plafker, J.D. Singer, S.M. Plafker, The ubiquitin conjugating enzyme, UbcM2, engages in novel interactions with components of cullin-3 based E3 ligases, Biochemistry 48 (2009) 3527–3537.

[36] S.M. Plafker, I.G. Macara, Importin-11, a nuclear import receptor for the ubiquitin-conjugating enzyme, UbcM2, EMBO J. 19 (2000) 5502–5513.

[37] S.M. Plafker, K.S. Plafker, A.M. Weissman, I.G. Macara, Ubiquitin charging of human class III ubiquitin-conjugating enzymes triggers their nuclear import, J. Cell Biol. 167 (2004) 649–659.

[38] J. Prudent, R. Zunino, A. Sugiura, S. Mattie, G.C. Shore, H.M. McBride, MAPL SUMOylation of Drp1 stabilizes an ER/mitochondrial platform required for cell death, Mol. Cell 59 (2015) 941–955.

[39] E. Riballo, M. Kuhne, N. Rief, A. Doherty, G.C. Smith, M.J. Recio, C. Reis, K. Dahm, A. Fricke, A. Krempler, et al., A pathway of double-strand break rejoining dependent upon ATM, Artemis, and proteins locating to gamma-H2AX foci, Mol. Cell 16 (2004) 715–724.

[40] E. Shvets, E. Fass, Z. Elazar, Utilizing flow cytometry to monitor autophagy in living mammalian cells, Autophagy 4 (2008) 621–628.

[41] J.D. Siliciano, C.E. Canman, Y. Taya, K. Sakaguchi, E. Appella, M.B. Kastan, DNA damage induces phosphorylation of the amino terminus of p53, Genes Dev. 11 (1997) 3471–3481.

[42] N. Sun, J. Yun, J. Liu, D. Malide, C. Liu, I.I. Rovira, K.M. Holmstrom, M.M. Fergusson, Y.H. Yoo, C.A. Combs, et al., Measuring In Vivo Mitophagy, Mol. Cell 60 (2015) 685–696.

[43] K.N. Swatek, D. Komander, Ubiquitin modifications, Cell Res. 26 (2016) 399–422.

[44] R.H. te Poele, A.L. Okorokov, L. Jardine, J. Cummings, S.P. Joel, DNA damage is able to induce senescence in tumor cells in vitro and in vivo, Cancer Res. 62 (2002) 1876–1883.
[45] M.P. Thome, E.C. Filippi-Chiela, E.S. Villodre, C.B. Migliavaca, G.R. Onzi, K.B. Felipe, G. Lenz, Ratiometric analysis of Acridine Orange staining in the study of acidic organelles and autophagy, J. Cell Sci. 129 (2016) 4622–4632.
[46] M.C. Velarde, J.M. Flynn, N.U. Day, S. Melov, J. Campisi, Mitochondrial oxidative stress caused by Sod2 deficiency promotes cellular senescence and aging phenotypes in the skin, Aging 4 (2012) 3–12.
[47] C.D. Wiley, J. Campisi, From ancient pathways to aging cells-connecting metabolism and cellular senescence, Cell Metab. 23 (2016) 1013–1021.
[48] C.D. Wiley, M.C. Velarde, P. Lecot, S. Liu, E.A. Sarnoski, A. Freund, K. Shirakawa, H.W. Lim, S.S. Davis, A. Ramanathan, et al., Mitochondrial dysfunction induces senescence with a distinct secretory phenotype, Cell Metab. 23 (2016) 303–314.
[49] R. Yau, M. Rape, The increasing complexity of the ubiquitin code, Nat. Cell Biol. 18 (2016) 579–586.
[50] Y. Ye, M. Rape, Building ubiquitin chains: E2 enzymes at work, Nat. Rev. Mol. Cell Biol. 10 (2009) 755–764.
[51] H. Zhao, H.D. Halicka, F. Traganos, E. Jorgensen, Z. Darzynkiewicz, New biomarkers probing depth of cell senescence assessed by laser scanning cytometry, Cytom. Part A: J. Int. Soc. Anal. Cytol. 77 (2010) 999–1007.